ON SPACE-TIME CODED ARTM CPM TO SOLVE THE TWO-ANTENNA PROBLEM

Michael Rice, Chad Josephson, Willie Harrison, Spencer Giddens
Department of Electrical & Computer Engineering
Brigham Young University
Provo, Utah, USA
mdr@byu.edu, chadcjosephson@gmail.com,
willie.harrison@byu.edu, giddens2spencer@gmail.com

Erik Perrins
Electrical Engineering and Computer Science Department
University of Kansas
Lawrence, Kansas, USA
esp@ku.edu

ABSTRACT

The space-time block code approach to solving the two-antenna problem is extended to ARTM CPM. The space-time block code is a block-based extension of the Alamouti space-time block code used in space-time coded SOQPSK-TG systems. A demodulator/decoder is described and analyzed both mathematically and in computer simulation. Without complexity reducing techniques, the decoder requires the Viterbi Algorithm operating on a trellis with 4,194,304 states. Complexity reduction techniques are applied to reduce the number of states to 256. Complexity reduction is accomplished at the cost of loss in detection efficiency that is a function of the differential delay between the space-time coded ARTM CPM signals transmitted from the two transmit antennas on the airborne test article.

INTRODUCTION

To increase the spatial coverage on fixed- and rotary-winged test articles, two antennas are often used to account for blockage by the fuselage. The most common configuration is to place one antenna on the top of the fuselage and the other on the bottom. The earliest implementations of this configuration transmitted the same RF telemetry signal from both antennas using a power splitter connected to the telemetry transmitter output. This implementation created a simple antenna array

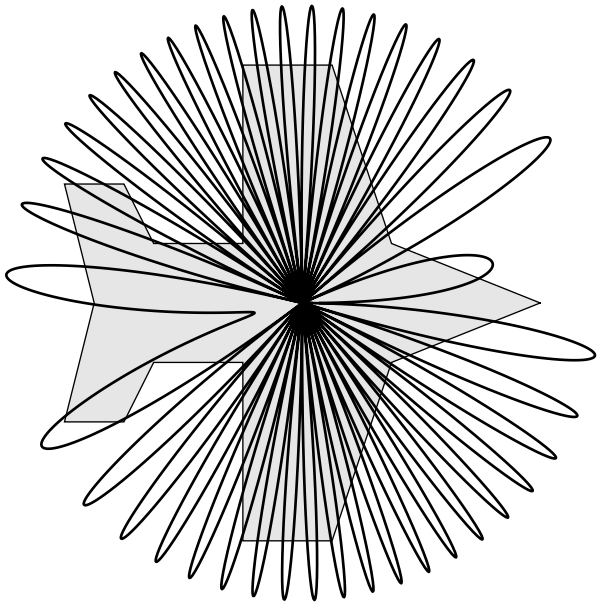

Figure 1: The azimuth slice of the gain pattern corresponding to transmitting the same signal from two antennas separated by 79.75 in. front-to-back, 16.5 in. left-to-right, and 69.5 in. top-to-bottom at L-band carrier frequency of 1485.5 MHz.

defined by the two antennas. An example of the radiation gain pattern created by two antennas is shown in Figure 1. Range engineers noticed signal drop outs during turns; the drop outs occurred when the propagation path from the test article to the ground station was through one of the nulls. As bit rates increased beyond 5 Mbits/s, range engineers experienced difficulties maintaining the link even when the propagation path was through one of the high-gain lobes. The link outages in this case were caused by self-interference resulting from the difference in propagation delays between the two antennas and the ground station. Collectively, the problems associated with transmitting the same signal from two antennas separated by several wavelengths is called the *two-antenna problem*.

The authors of [1] (see also the ITC paper [2]) showed that orthogonal space-time block codes can solve the two-antenna problem. Based on the theoretical analysis of [1], modulator and demodulator/decoder prototypes were developed for SOQPSK-TG using the Alamouti space-time block code [3]. The success of the flight tests [4, 5] prompted the development of commercially-available space-time coded SOQPSK-TG systems [6, 7, 8, 9].

In this paper, the space-time code solution to the two-antenna problem is extended to ARTM CPM. Because of the differences between SOQPSK-TG and ARTM CPM, a different space-time code must be used. This code is described in the next section. The demodulator/decoder is described in the section after.

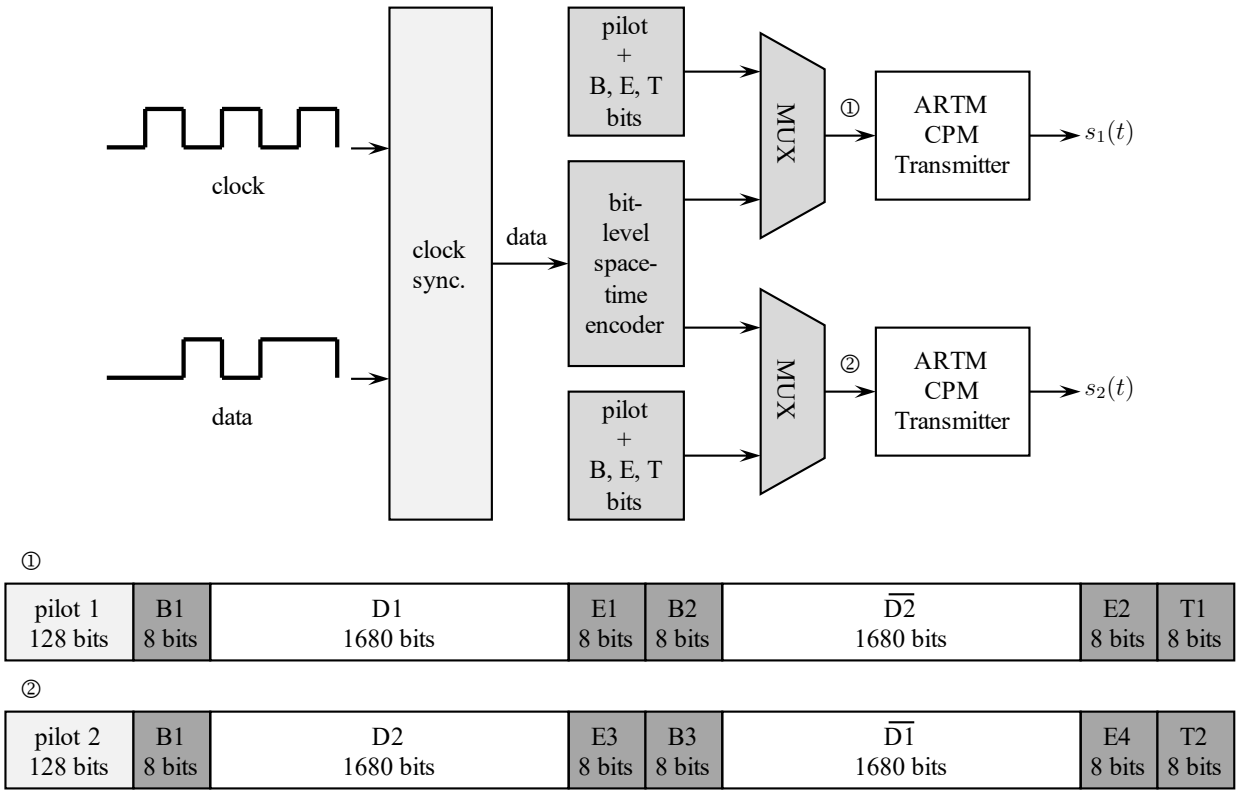

Figure 2: A conceptual block diagram of a space-time coded transmitter.

SPACE-TIME BLOCK CODE

The space-time coded transmitter has a single input data stream and produces two RF ARTM CPM signals, one for each transmit antenna. The space-time coded ARTM CPM signals are of the form

$$\begin{aligned} s_1(t) &= A\cos(2\pi f_c t + \phi_1(t)) \\ s_2(t) &= A\cos(2\pi f_c t + \phi_2(t)) \end{aligned} \tag{1}$$

where A is the amplitude of the RF waveform (determined by the transmitter power), f_c is the carrier frequency, and $\phi_1(t)$ and $\phi_2(t)$ are the time-varying phases that describe ARTM CPM.

A block diagram of the space-time coded ARTM CPM transmitter is shown in Figure 2. The transmitter comprises one input data stream, a bit-level space time encoder, the insertion of bit fields needed to enable space-time decoding, and a pair of transmitters. A description of the inputs to the two parallel transmitters is also shown in the figure.

The space-time encoder is based on the space-time block code for CPM developed by Silvester [10]. Consecutive blocks of 3360 bits are partitioned into two non-overlapping parts, called "D1" and "D2", each with 1680 bits. During the first half of the transmission the ARTM CPM signal corresponding to "D1" is sent from antenna 1 while the ARTM CPM signal corresponding to "D2" is sent from antenna 2. During the second half of the block, the negative of the ARTM CPM signal

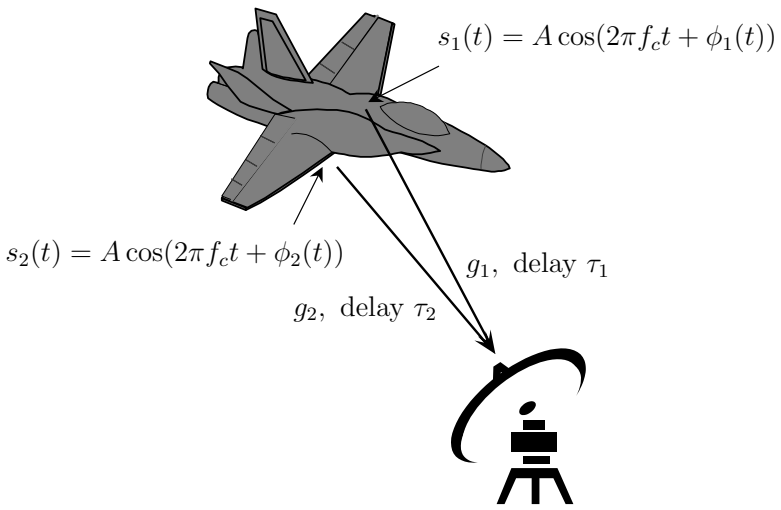

$$r(t) = g_1 A\cos(2\pi(f_c + \Delta f)(t - \tau_1) + \phi_1(t) + \gamma_1) + g_2 A\cos(2\pi(f_c + \Delta f)(t - \tau_2) + \phi_2(t) + \gamma_2) + n(t)$$

Figure 3: A system-level diagram describing the space-time coded ARTM CPM system.

corresponding to "$\overline{\mathrm{D2}}$" is sent from antenna 1 while the ARTM CPM signal corresponding to "$\overline{\mathrm{D1}}$" is sent from antenna 2 where the horizontal line means logical complement. For readers familiar with the Alamouti space-time block code [3], the block-based encoding strategy used here is the extension of the symbol-based Alamouti code to a data block.

The "B", "E", and "T" bit fields are required to initialize, end, or terminate the trellis that describes the ARTM CPM waveform state. This is required because of the way the demodulator combines the first half and second half of the received block to perform space-time decoding.

The pilot bits are inserted before each block to allow the demodulator to estimate the propagation parameters required for optimum detection. This is described in the next section.

The ratio of output bits to input bits on each of the two parallel channels is

$$\frac{128 + 8 + 1680 + 8 + 8 + 1680 + 8 + 8}{1680 + 1680} = \frac{21}{20}. \tag{2}$$

In words, the over-the-air bit rate is 21/20 times the user bit rate, or 5% higher. The 5% increase represents the overhead required to enable space-time coding.

DEMODULATOR/DETECTOR

A system-level block diagram of a space-time encoded ARTM CPM system is presented in Figure 3. The received signal is

$$r(t) = g_1 A \cos(2\pi(f_c + \Delta f)(t - \tau_1) + \phi_1(t) + \gamma_1) + g_2 A \cos(2\pi(f_c + \Delta f)(t - \tau_2) + \phi_2(t) + \gamma_2) + n(t) \quad (3)$$

where

$g_1 =$ the gain of the propagation path from transmitter output 1 to the ground station. This gain includes cable and connector losses between the transmitter and antenna 1, the gain of the antenna 1 in the direction of the ground station, the spreading loss, and the gain of the receive antenna.

$g_2 =$ the gain of the propagation path from transmitter output 2 to the ground station. This gain includes cable and connector losses between the transmitter and antenna 2, the gain of the antenna 2 in the direction of the ground station, the spreading loss, and the gain of the receive antenna.

$\tau_1 =$ the propagation delay between transmitter output 1 and the ground station. This includes any delays due to cabling.

$\tau_2 =$ the propagation delay between transmitter output 2 and the ground station. This includes any delays due to cabling.

$\gamma_1 =$ the phase shift associated with the propagation path between transmitter output 1 and the ground station.

$\gamma_2 =$ the phase shift associated with the propagation path between transmitter output 2 and the ground station.

$\Delta f =$ the frequency offset. The frequency offset is a combination of oscillator uncertainty and Doppler shift.

$n(t) =$ the thermal noise generated primarily by the LNA and antenna feed electronics in the receive antenna. The thermal noise is modeled as a white normal random process with power spectral density $N_0/2$ W/Hz.

To perform optimal decoding, the space-time decoder must have good estimates of g_1, g_2, τ_1, τ_2, γ_1 and γ_2. These parameters are estimated from the received signal samples corresponding to the ARTM CPM waveforms carrying the pilot bits. The decoder does not need to know the frequency offset Δf *per se*, but assumes the frequency offset has been removed prior to decoding.

A block diagram of the space-time demodulator/decoder is illustrated in Figure 4. The received signal $r(t)$ is the real-valued bandpass RF signal produced by the ground station antenna. The mathematical expression is given by (3). The received RF signal is filtered, amplified, and converted to a 70 MHz RF signal by a telemetry receiver. The IF signal is sampled by an A/D converter

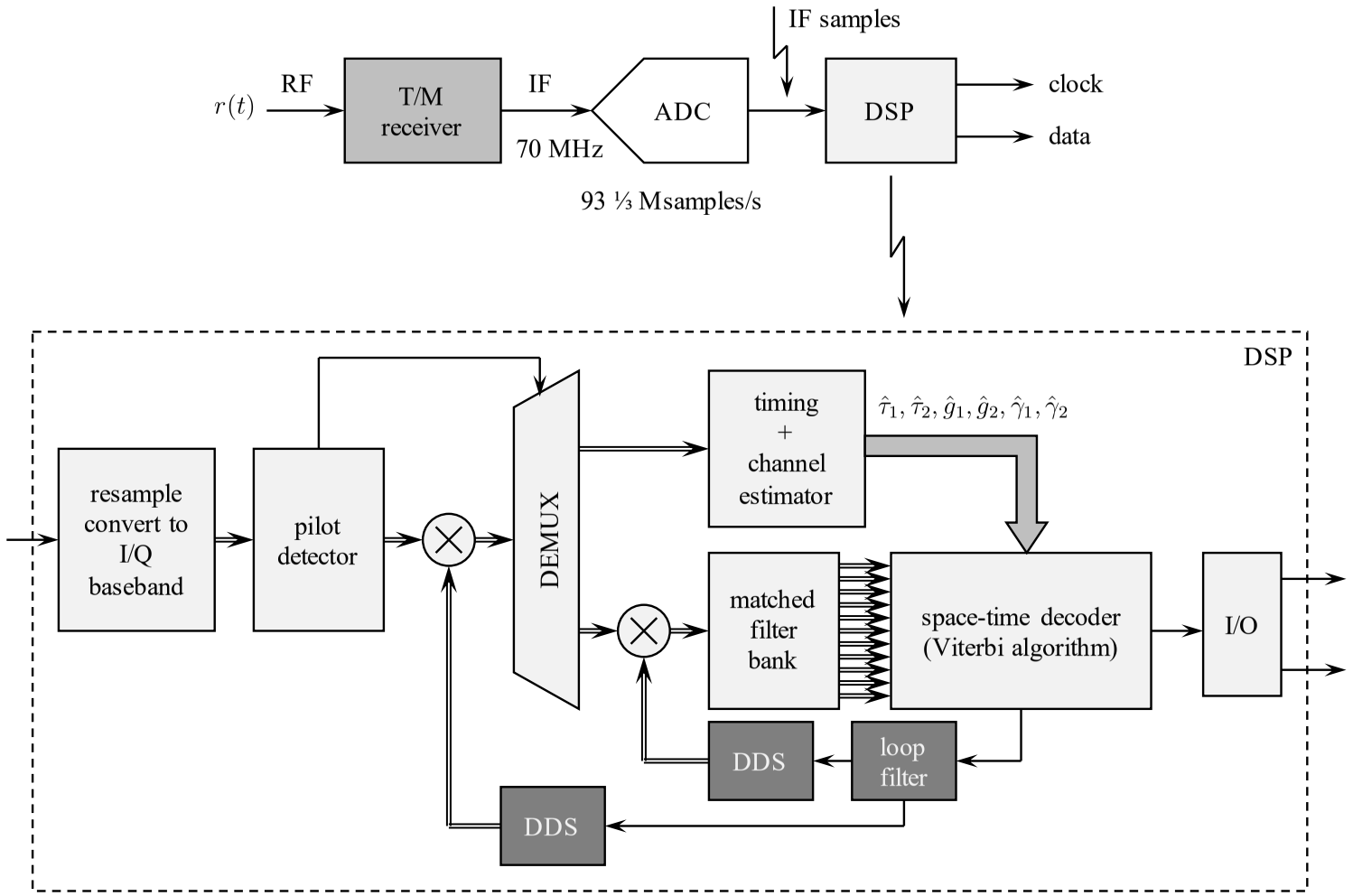

Figure 4: A system-level block diagram of the demodulator/decoder for space-time coded ARTM CPM.

(ADC in the figure) operating at 93 $1/3$ Msamples/s. The reason for this sample rate is described in Chapter 10 of [11]. Synchronization and decoding are achieved using the IF samples in the "DSP" block. The major components of the DSP block are described in the following subsections.

A. RESAMPLING AND CONVERSION TO I/Q BASEBAND

Resampling filters, in the form of two cascaded polyphase filterbanks perform simultaneous resampling and frequency translation to I/Q baseband. The purpose of resampling is to produce an equivalent sample rate of 4 samples/symbol (= 2 samples/bit), where the reference bit rate is the over-the-air bit rate. The use of polyphase filterbanks for resampling and frequency translation is described in Chapter 10 of [11].

B. PILOT DETECTOR

The role of the pilot detector is to find the location of the I/Q ARTM CPM waveform samples corresponding to the pilot bits. The location is determined by computing a pair of semi-coherent cross-correlations between the received I/Q samples and locally stored copies of I/Q samples of the ARTM CPM waveform corresponding to the two pilot bit sequences. Note that both the I/Q samples and the locally stored copies are sampled at a rate equivalent to 2 samples/bit.

The correlation peaks identify the occurrence of the pilot samples in the received I/Q samples. The location of the pilot samples controls a DEMUX operation that routes the 256 I/Q samples corresponding to the pilots to the channel and timing estimator and the remainder of the I/Q samples to the decoder.

C. TIMING AND CHANNEL ESTIMATOR

The timing and channel estimator computes estimates of τ_1, τ_2 (the "timing estimates") along with estimates of g_1, g_2, γ_1, and γ_2 (the "channel estimates"). The estimates are denoted using the "hats" in Figure 4. The estimates are produced in two steps. In the first step, $\hat{\tau}_1$ and $\hat{\tau}_2$ are computed by solving

$$\hat{\tau}_1, \hat{\tau}_2 = \underset{\tau_1,\tau_2}{\operatorname{argmin}} \left\{ \left| \left[\mathbf{I} - \mathbf{P}(\tau_1,\tau_2) \left(\mathbf{P}^H(\tau_1,\tau_2)\mathbf{P}(\tau_1,\tau_2) \right)^{-1} \mathbf{P}^H(\tau_1,\tau_2) \right] \tilde{\mathbf{r}} \right|^2 \right\} \tag{4}$$

where $\mathbf{I}$ is the 256×256 identity matrix; $\mathbf{P}(\tau_1, \tau_2)$ is a 256×2 matrix where the first and second columns contain I/Q samples of the ARTM CPM waveform corresponding to pilot 1 and pilot 2, respectively, where the samples are delayed by τ_1 and τ_2, respectively; $\tilde{\mathbf{r}}$ is the 256×1 vector of received I/Q samples after de-rotation by the outer loop (see subsection F); and $(\cdot)^H$ is the Hermitian (conjugate-transpose) matrix/vector operation. The solution to (4) is obtained by the gradient-descent method described in [12].

After computing the delay estimates $\hat{\tau}_1$ and $\hat{\tau}_2$, the complex-valued channel gains are computed using

$$\begin{bmatrix} \hat{\mathbb{g}}_1 \\ \hat{\mathbb{g}}_2 \end{bmatrix} = \left(\mathbf{P}^H(\hat{\tau}_1, \hat{\tau}_2) \mathbf{P}(\hat{\tau}_1, \hat{\tau}_2) \right)^{-1} \mathbf{P}^H(\hat{\tau}_1, \hat{\tau}_2) \tilde{\mathbf{r}}. \tag{5}$$

where $\mathbb{g}_1 = g_1 e^{j\gamma_1}$ and $\mathbb{g}_2 = g_2 e^{j\gamma_2}$. Note that the matrix product involving $\mathbf{P}(\hat{\tau}_1, \hat{\tau}_2)$ in (5) is computed during the search (4) and does not need to be recomputed to produce the channel estimates.

D. DECODER

The maximum likelihood space-time decoder is based on the maximum likelihood detector for uncoded ARTM CPM [13]. The maximum likelihood detector comprises a bank of correlators (called matched filters) followed by a maximum likelihood sequence estimator. The algorithm used to perform maximum likelihood sequence estimation is the Viterbi Algorithm. The Viterbi Algorithm operates on a trellis defined by the possible signal states during each symbol (two-bit) interval. The complete representation of ARTM CPM requires 512 states. It is the authors' understanding that most commercially available ARTM CPM detectors apply some of the reduced state techniques described in [13] to create a trellis with a smaller number of states. The state reduction is achieved at the cost of a modest reduction in detection efficiency.

The space-time decoder operates on the same principles. Incorporating the space-time code and the differential delay between $s_1(t)$ and $s_2(t)$, a super-trellis comprising 4,194,304 states is required. Clearly, this is far too large to be implemented in a practical system. By applying the pulse truncation (PT) and state-space partitioning (SSP) state reduction techniques described in [13] to the decoding problem, the number of states can be reduced to 256 states [14].

The detection efficiency associated with the state reduction techniques is illustrated by the probability of bit error curves shown in Figure 5. Observations:

1. The full complexity decoder achieves the same bit error probability performance as the uncoded ARTM CPM system with a full complexity detector (not shown to reduce clutter).

2. The decoder based only on PT—this produces a trellis with 65,536 states—does not produce any measurable loss in detection efficiency. This is hard to see in the plot: the light gray line (full complexity) and the medium gray dashed line (PT) are on top of each other.

3. The decoder based on PT+SSP—this produces the 256-state trellis—is characterized by a detection efficiency that decreases with increasing $|\Delta\tau|$. The mathematical analysis predicts losses in detection efficiency at $P_b = 10^{-6}$ of 0.6 dB for $\Delta\tau = 0$, 1.4 dB for $\Delta\tau = 0.3T_s$, 2.5 dB for $\Delta\tau = 0.6T_s$, and 3 dB for $\Delta\tau = 0.9T_s$. The computer simulations produce probability of bit error estimates that match or are within 0.25 dB of the mathematical analysis.

The interesting observation is that the full complexity decoder and PT decoder show no variation

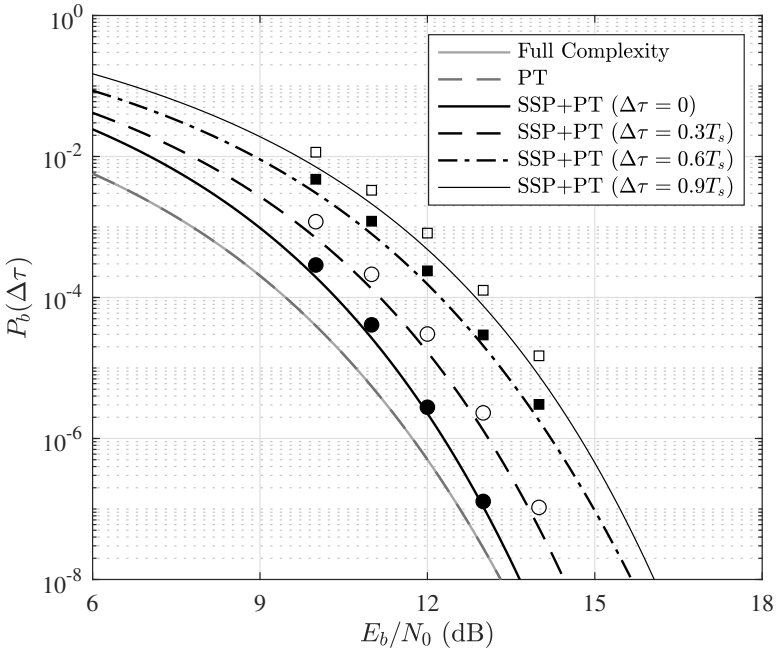

Figure 5: Probability of bit error vs. E_b/N_0 for the full complexity decoder, the reduced complexity decoder using PT, and the reduced complexity decoder using PT + SSP for $g_1 = 1$, $g_2 = -1$, and for various values of $\Delta\tau = \tau_1 - \tau_2$. Computer simulations of the bit error probability for the decoder with PT + SSP are shown by the markers. Reproduced from [14].

in the probability of bit error with $\Delta\tau$. The variation of the probability of bit error with $\Delta\tau$ is a byproduct of the SSP complexity reduction.

E. FREQUENCY OFFSET COMPENSATION

Frequency offset is caused by a combination of oscillator uncertainty and Doppler shift. The system was designed to accomodate frequency offsets in the range $\Delta f = \pm 30$ kHz. Frequency offset compensation took the form of two closed loop systems. The elements of these closed-loop systems are shown by the dark gray boxes in Figure 4. These closed loop systems are called the "inner loop" and "outer loop."

The inner loop is a PLL designed to track out the phase increment/decrement due to a small error in the current frequency estimate. The PLL derives its error from tentative decisions in the Viterbi Algorithm as described in [15]. The error signal is filtered by a loop filter that drives a direct digital synthesizer (DDS) that closes at the input to the matched filter bank. The loop filter is a discrete-time proportional-plus-integrator filter. Consequently, the output of the loop filter is an estimate of the residual frequency offset seen by the inner loop. The output of the loop filter at the end of each block is used to update the outer loop.

The outer loop is a frequency lock loop (FLL) designed to track out the frequency offset in the

received I/Q samples. The FLL comprises a DDS that closes at the output of the pilot detector. (The FLL should close at the input to the pilot detector. For reasons relating to the FPGA implementation [an ongoing process as of this writing] the FLL closes at the output of the pilot detector.) The oscillation frequency of the DDS is updated once per block using the output of the loop filter in the inner loop as described in the previous paragraph.

CONCLUSIONS

The use of space-time block coding to solve the two-antenna problem has been extended to ARTM CPM. The space-time block code is a block-based extension of the symbol-based Alamouti space-time code used in space-time coded SOQPSK-TG systems. A demodulator/decoder has been designed and analyzed both mathematically and in computer simulation. The results show that the complexity reductions required to make the implementation feasible produce a detection efficiency loss that increases with the differential delay. An FPGA implementation of the demodulator/detector is an ongoing effort.

ACKNOWLEDGEMENTS

This project is managed by the Test Resource Management Center (TRMC) and funded through Spectrum Access R&D Program via Picatinny Arsenal under Contract No. W15QKN-15-9-1004.

REFERENCES

[1] M. Jensen, M. Rice, and A. Anderson, "Aeronautical telemetry using multiple-antenna transmitters," *IEEE Transactions on Aerospace and Electronic Systems*, vol. 43, no. 1, pp. 262–272, January 2007.

[2] M. Jensen, M. Rice, T. Nelson, and A. Anderson, "Orthogonal dual-antenna transmit diversity for SOQPSK in aeronautical telemetry channels," in *Proceedings of the International Telemetering Conference*, San Diego, CA, October 2004, pp. 337–344.

[3] S. Alamouti, "A simple transmit diversity technique for wireless communications," *IEEE Journal on Selected Areas in Communications*, vol. 16, no. 8, pp. 1451–1458, October 1998.

[4] M. Rice, J. Palmer, C. Lavin, and T. Nelson, "Space-time coding for aeronautical telemetry: Part I—estimators," *IEEE Transactions on Aerospace and Electronic Systems*, vol. 53, no. 4, pp. 1709–1731, August 2017.

[5] M. Rice, T. Nelson, J. Palmer, C. Lavin, and K. Temple, "Space-time coding for aeronautical telemetry: Part II——decoder and system performance," *IEEE Transactions on Aerospace and Electronic Systems*, vol. 53, no. 4, pp. 1732–1754, August 2017.

[6] Quasonix Space Time Coding (STC) System. Quasonix. [Online]. Available: https://www.quasonix.com/files/receiver-and-transmitter-space-time-coding-datasheet.pdf

[7] SEMCO R100A Series Telemetry Receiver. SEMCO. [Online]. Available: https://www.semco.com/wp-content/uploads/R100ASeries.pdf

[8] RX-1 Compact Telemetry Receiver. Safran Data Systems. [Online]. Available: https://www.safrandatasystemsus.com/datasheets/Telemetry/RX-1_Datasheet.pdf

[9] TTC TTS-9800-2 Airborne Multi-Band Multimode Transmitter. Curtiss-Wright. [Online]. Available: https://www.curtisswrightds.com/products/flight-test/radio-frequency/tts98002.html

[10] A. Silvester, R. Schober, and L. Lampe, "Burst-based orthogonal ST block coding for CPM," *IEEE Transactions on Wireless Communications*, vol. 6, no. 4, pp. 1208–1212, April 2007.

[11] M. Rice, *Digital Communications: A Discrete-Time Approach*. Kindle Direct Publishing, Amazon.com, 2018, ISBN-13: 978-0-13-030497-1.

[12] S. Giddens, "Applications of Mathematical Optimization Methods to Digital Communications and Signal Processing," Master's thesis, Brigham Young University, 2020. [Online]. Available: http://hdl.lib.byu.edu/1877/etd11348

[13] E. Perrins and M. Rice, "Reduced-complexity detectors for multi-h CPM in aeronautical telemetry," *IEEE Transactions on Aerospace and Electronic Systems*, vol. 43, no. 1, pp. 286–300, January 2007.

[14] C. Josephson, E. Perrins, and M. Rice, "Space-time block coded ARTM CPM for aeronautical mobile telemetry," to appear in *IEEE Transactions on Aerospace and Electronic Systems*, 2021.

[15] U. Mengali and A. D'Andrea, *Synchronization Techniques for Digital Receivers*. New York: Springer Science+Business Media, 1997, ISBN-13: 978-0306457258.